Transport-Limited Recombination of Photocarriers in Dye-Sensitized Nanocrystalline TiO_2 Solar Cells

Nikos Kopidakis, Kurt D. Benkstein, Jao van de Lagemaat, and Arthur J. Frank*

National Renewable Energy Laboratory, Golden, Colorado 80401

Received: April 16, 2003

The effect of lithium intercalation on the transport dynamics and recombination kinetics in dye-sensitized nanoparticle TiO_2 solar cells at lithium levels below 5 atom % was investigated by photocurrent and photovoltage transient and spectroelectrochemical techniques. Titanium dioxide films were doped electrochemically in the dark and under illumination. It was discovered that when Li^+ is present in the electrolyte, lithium intercalates irreversibly into dye-sensitized TiO_2 films at open circuit (ca. −0.7 V) under normal solar light intensities. Photocurrent transients of doped nonsensitized TiO_2 films indicate that lithium doping decreases the diffusion coefficient of electrons through the nanoparticle network. Photocurrent and photovoltage transients of sensitized TiO_2 films provide the first evidence that electron transport limits recombination with the redox electrolyte in working cells. As the Li density in the films increases, the diffusion and recombination times of photoelectrons increase proportionately, indicating a causal link between electron transport and recombination. The electron diffusion coefficient in dye-sensitized solar cells exhibits a power-law dependence on photocharge at all concentrations of inserted lithium in the TiO_2 film. With increasing doping, the dependence of the electron diffusion coefficient on the photocharge becomes stronger, a phenomenon attributed to widening of the exponential conduction band tail resulting from disorder induced by randomly placed lithium defects in TiO_2. The photovoltaic characteristics of dye-sensitized solar cells are largely unaffected by lithium intercalation, implying that intercalation has only a small effect on the charge collection efficiency and the rate of recombination. A simple model is presented that explains the observed transport-limited recombination. The results suggest that increasing the electron transport rate will not significantly improve the solar cell performance.

Introduction

The electron transport dynamics and recombination kinetics are major determinants of the overall efficiency of dye-sensitized nanocrystalline TiO_2 solar cells (Grätzel cell; DSSCs). Following their injection into the conduction band of TiO_2 by photoexcited dye molecules adsorbed to the nanoparticle surface, electrons travel through the TiO_2 film, where they are collected at the back contact (collecting electrode) unless they recombine with redox species (e.g., I_3^-) in the electrolyte. Redox species in the electrolyte transport the holes from the oxidized dye molecules to the counter electrode. The transport of injected electrons to the collecting electrode occurs almost exclusively by diffusion because the *macroscopic* electric fields across the cell are screened by the electrolyte at normal solar light intensities.[1−6] Because of electrostatic interaction of the electrons in the TiO_2 with the ions in the electrolyte, their diffusion is ambipolar (i.e., coupled).[1,7−9] The electron transport dynamics have been studied by transient photocurrent measurements,[1,7,10−16] intensity-modulated photocurrent spectroscopy,[2,12,17−23] electrical impedance spectroscopy,[2,15,24−26] and current−voltage measurements.[15,27−30] The diffusion of electrons through the nanoparticle network is several orders of magnitude slower than that in single-crystal TiO_2[1,16] and is nonlinearly dependent on the concentration of photoinjected electrons in the films.[1,2,7,17,18,23] The slow nonlinear transport dynamics have been explained by assuming trap-limited transport involving an exponential distribution of localized trap states adjacent to the conduction band edge.[1,7,17,18,23,28,31,32]

Recombination in DSSCs has been studied by time-resolved optical absorption,[33−35] intensity-modulated photovoltage spectroscopy,[2,32,36] and time-resolved photovoltage transients.[37] A remarkable property of DSSCs, which is a key to their relatively high efficiency, is that recombination of photoinjected electrons with I_3^- in the liquid electrolyte is extremely slow.[1,36] Moreover, the rate of recombination depends nonlinearly on the electron concentration,[19,32,36] as in the case of the electron transport dynamics, which leads to an electron collection efficiency and electron diffusion length that are almost independent of light intensity.[32] The nonlinear recombination kinetics have been explained in terms of an exponential trap distribution model, as in the case of the electron transport dynamics, combined with a model based on the complex iodine reduction chemistry at the TiO_2 surface.[32,36] In the absence of redox species in the electrolyte, the recombination of photoinjected electrons takes place with the oxidized dye molecules—instead of iodine—and follows nonlinear kinetics, a phenomenon that has been attributed to transport-limited recombination in which transport is slowed by the presence of exponentially distributed traps.[33−35] However, in a working DSSC, incorporating a redox electrolyte, the recombination of photoinjected electrons with oxidized dye molecules is negligible except at high electron densities produced by very negative applied biases[33] or very high light intensities.[34]

Phenomena at the TiO_2 particle surface have a significant influence on the cell performance. Treating the TiO_2 surface

* Corresponding author.

10.1021/jp0304475 CCC: $25.00
Published on Web 09/19/2003

with 4-*tert*-butyl pyridine is found[36] to shift the conduction band edge to more negative potential, which increases the open-circuit voltage. Adsorption of Li^+ ions from the electrolyte to the TiO_2 surface increases the charge injection efficiency of the excited state of the dye by shifting the conduction band edge to more positive potentials.[38−40]

Because of its relevance to electrochromics and batteries, the mechanism of lithium insertion (intercalation) into anatase TiO_2 has been studied extensively.[41−49] The electrochemical intercalation of lithium is believed to be driven by the accumulation of electrons in TiO_2 electrodes in contact with Li^+ containing electrolytes.[43,45−48]

$$x\mathrm{Li}^+ + x\mathrm{e}_{\mathrm{TiO_2}}^- + \mathrm{TiO_2} \rightharpoonup \mathrm{Li}_x\mathrm{TiO_2} \qquad (1)$$

where $e_{TiO_2}^-$ represents electrons in TiO_2. This reaction is considered to be reversible. When the density of inserted Li exceeds about 5 atom %,[43,49] the solid solution of Li in anatase TiO_2 (Li:TiO_2) undergoes a transformation to lithium titanate (Li_xTiO_2). This phase transformation is paired with a considerable change in optical absorption, which is the basis for the use of anatase TiO_2 in electrochromics. The highest Li uptake in nanocrystalline TiO_2 is reported to be about 50 atom %.[49] Lithium titanate converts reversibly back to the solid solution of Li in anatase TiO_2 when Li is deintercalated below 5 atom %.[43] However, once transformed at 5 atom %, Li cannot be extracted completely from the solid solution by cycling the voltage several times.[41] Residual Li is presumed to reside in domains of the TiO_2 film that underwent the phase transformation.[45] Irreversible deposition of lithium compounds (e.g., LiOH) on the nanocrystalline TiO_2 surface can also occur during voltage cycling.[42] The lithium intercalation−deintercalation history of a TiO_2 film strongly influences its electrical conductivity.[44] The overall conductivity of the film drops significantly, by a factor of 2, after a single insertion−extraction cycle.[44]

In this paper, we explore the effect of lithium intercalation on the transport dynamics and recombination kinetics in dye-sensitized solar cells at lithium densities below 5 atom %. It is shown for the first time that electron transport limits recombination in working cells. Irreversible lithium insertion is found to slow dramatically both transport and recombination. It is discovered that lithium insertion occurs under the normal operating conditions of a cell containing a lithium electrolyte. The implications of lithium intercalation on the photovoltaic (PV) characteristics of the DSSC were also investigated.

Experimental Section

Sample Preparation. TiO_2 nanoparticles were prepared and analyzed as previously described.[2,50,51] The preparation method yields exclusively anatase TiO_2 with a narrow size distribution centered at a particle diameter of 19 nm. The TiO_2 paste was spread on top of a conducting glass plate (LOF TEC8 F-doped SnO_2 glass; Hartford Glass Company), which was used as the substrate for the deposited films. Transparent adhesive tape (nominal thickness 40 μm) was used as a spacer to control the film thickness, which ranged from 4 to 10 μm. The porosity of the films was about 62%. The TiO_2-covered glass was sintered in air at 450 °C for 30 min and then allowed to cool. For dye-sensitization studies, the annealed TiO_2 electrodes were immersed in ethanol containing 3×10^{-4} M Ru[LL′(NCS)$_2$] (L = 2,2′-bypyridyl-4,4′-dicarboxylic acid, L′ = 2,2′-bipyridyl-4,4′-ditetrabutylammoniumcarboxylate) for 24 h at room temperature. The dye-covered electrodes were then rinsed with absolute ethanol and dried under a N_2 stream. To minimize rehydration of TiO_2 from moisture in the ambient air, the electrodes were immersed in the dye solution while they were still warm (100−120 °C) from the annealing step. In some studies, the films were electrochemically doped with lithium and rinsed with ethanol before being exposed to the dye solution. Table 1 summarizes the procedure used in electrochemically doping the TiO_2 films with lithium. In one case (Sample #6; Table 1), the sensitized film was exposed to 4-*tert*-butyl pyridine.[36] The active area of the films was 0.15−0.25 cm^2. Semitransparent counter electrodes were prepared by spreading a droplet of 5 mM H_2PtCl_6 in 2-propanol onto TEC8 conducting glass plates and subsequently firing them at 350 °C for 40 min. The cells used for the dye-sensitization studies were filled with one of the two following redox electrolytes in distilled methoxypropionitrile: 0.8 M 1-hexyl-2,3-dimethylimidazolium iodide (C6DMII) with 50 mM iodine or 0.8 M LiI with 50 mM iodine. All solar cells were assembled as described elsewhere.[7]

TABLE 1: Experimental Conditions for Intercalating Lithium into TiO_2 Nanoparticle Films[a]

cell #	electrode treatment before studies	electrolyte composition[b]
1	dye-stained TiO_2 not exposed to a lithium electrolyte	0.8 M C6DMII/0.05 M I_2
2	TiO_2 cycled once between 0 and −1.3 V before dye staining	0.8 M C6DMII/0.05 M I_2
3	TiO_2 in 0.5 M $LiClO_4$/acetonitrile cycled (3 mV/s)[d] 0 to −0.6 V, 0 to −0.8, 0 to −1.0 V, and 0 to −1.5 V before dye staining	0.8 M C6DMII/0.05 M I_2
4	TiO_2 in 0.5 M $LiClO_4$/acetonitrile cycled four times (6 mV/s) between 0 and −1.5 V before dye staining	0.8 M C6DMII/0.05 M I_2
5	dye-stained TiO_2 exposed to light[c] at open circuit for total of 0 min,30 min, and $3\frac{1}{2}$ h before transient measurement	0.8 M LiI/0.05 M I_2
6	4-*tert*-butylpyridine-treated dye-stained TiO_2 exposed to light[c] at open circuit for a total of 0 min, 30 min, 5 1/2 h, and 3 days 5 1/2 h before transient measurement	0.8 M LiI/0.05 M I_2

[a] Potential vs Ag/AgCl reference electrode. [b] Methoxypropionitrile was used as the solvent for sensitization studies. [c] AM1.5 equivalent light. [d] Most negative potential (−1.5 V) determines the upper density of inserted Li (see discussion of Figure 4).

Measurements on Nonsensitized TiO_2. Single-compartment three-electrode cells, consisting of a nonsensitized mesoporous nanoparticle TiO_2 working electrode, a Pt foil counter electrode, and a Ag/AgCl wire reference electrode were used for electrochemical and photocurrent transient measurements. The edges of the TiO_2 film were covered with a resin or with a rubber O-ring to limit exposing the SnO_2 substrate to the electrolyte, which was composed of 0.5 M $LiClO_4$ in acetonitrile. For electrochemical studies, voltage control and current measurements utilized an EG&G model 283 potentiostat. For spectroelectrochemical measurements, an Agilent model 8453 UV−vis spectrophotometer was also utilized, and the three electrodes were inserted into a quartz cuvette. For UV photocurrent transient measurements, TiO_2 electrodes were probed with 337 nm radiation from a N_2 pulsed laser in the absence of bias light.

Measurements on Assembled DSSCs. For transient photocurrent and photovoltage studies of DSSCs, the cells were probed with a weak laser pulse at 532 nm superimposed on a relatively large, background (bias) illumination at 680 nm. The bias light was incident on the cell from the collecting electrode (substrate) side. The bias light was supplied by a 0.5 W SDL model 7421 H1 laser-diode. The intensity of the bias light was varied using neutral density filters. The 680 nm bias light is only weakly absorbed by the dye (the effective absorption coefficient of the cell is about 500 cm^{-1} for 680 nm light) and

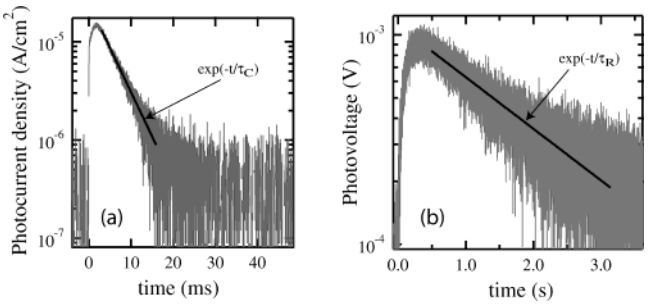

Figure 1. Photocurrent (a) and photovoltage (b) transient for a DSSC induced by the 532 nm probe pulse superimposed on the 680 nm bias light. The lines indicate the fit with exponential decay functions. The bias light generated (a) a short-circuit current of 1.4 mA/cm^2 and (b) an open circuit voltage of 0.4 V. The respective probe pulses and bias light were incident on the cell from the collecting electrode side and the counter-electrode side. The TiO_2 film was 6 μm thick.

therefore provides a relatively constant and approximately homogeneous electron-injection current throughout the film. The probe laser pulses were generated by a 30 mW frequency-doubled Nd:YAG laser (Laser compact Co. LCS-DTL-112QT) (λ = 532 nm, pulse duration 10 ns). The probe laser pulses were incident from the counter-electrode side. The 532 nm probe light is strongly absorbed by the dye (the effective absorption coefficient of the cell is about 5×10^3 cm^{-1} at 532 nm) and therefore the injected electrons are introduced into a narrow spatial region of the film, corresponding to where the probe light enters the film. The current transients were measured using a Stanford Research Systems model SR570 low-noise current preamplifier, amplified by a Stanford Research Systems model SR560 low-noise preamplifier, and recorded on a LeCroy 9350A 500 MHz oscilloscope. The transient photovoltage signal was amplified with the Stanford Research Systems model SR560 low-noise preamplifier. The response time of the preamplifier at the range of photocurrents used was less than 1 μs. The light intensity of the probe light was adjusted so that the collected charge induced by the probe light was less than 1% of the steady-state charge as estimated from the product of the steady-state short-circuit photocurrent and the time constant for electron collection.

Photocurrent and Photovoltage Transient Analysis of DSSCs. The characteristic times for electron diffusion (collection) and electron recombination in the cell were measured by photocurrent and photovoltage transients induced by a small probe pulse superimposed on a large steady-state bias light (Figure 1). Both the photocurrent and photovoltage decay exponentially with characteristic time constants that are independent of the probe pulse intensity. The characteristic times depend on the photocarrier density N in the film established by the bias light.[1,2,7,17,18,23,36] Although the photocurrent and photovoltage decay is due to a small density of additional photocarriers produced in the film by the probe pulse, the measured time constants are averages for the arrival times or recombination times for all electrons that contribute to the photocurrent or the recombination current. In the photocurrent transient measurements, the characteristic time constant (or collection time) τ_C represents the average time of the photoinjected electrons in the ensemble to diffuse to the collecting electrode at short circuit. The diffusion coefficient D can be estimated from the collection time τ_C with the expression[7]

$$D = d^2/(2.35\tau_C) \qquad (2)$$

where d is the film thickness. It would be more correct to refer to D as the ambipolar diffusion coefficient.[1] However, because the electron concentration in TiO_2 films is much less than the ion concentration in the liquid electrolyte, the ambipolar diffusion coefficient is, to a very good approximation, the same as the diffusion coefficient of electrons in the mesoporous network.[1] The photocarrier density N, induced by the bias light in a film of porosity P, is estimated from the collection time (or diffusion time) τ_C with the equation[1,7,23,36]

$$N = J_{SC}\tau_C/(q_e d(1 - P)) \qquad (3)$$

where J_{SC} is the short-circuit photocurrent density at different (bias) light intensities and q_e is the unit of charge of an electron; J_{SC} is proportional to the light intensity. This equation follows from the definition of current as the number of charges arriving at the collecting electrode per unit time and only assumes that the recombination current at short circuit is negligible.

In the photovoltage transient measurements, which are measured at open circuit, the characteristic time constant τ_R represents the recombination lifetime of electrons at the steady-state photocarrier density N. This lifetime is identical to that obtained by intensity-modulated photovoltage spectroscopy.[36] The photocarrier density at open circuit can be calculated by replacing τ_C in eq 3 with τ_R.

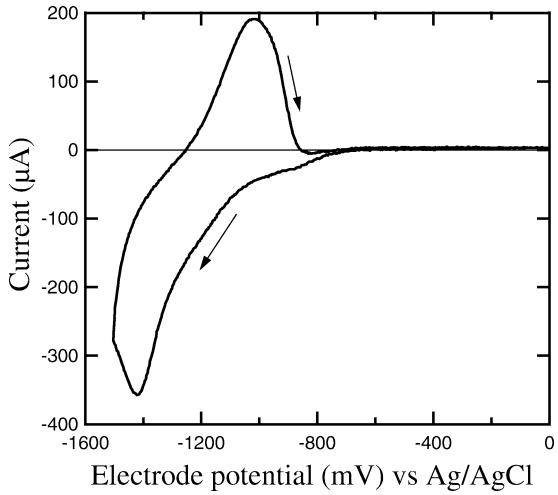

Figure 2. Cyclic voltammogram (6 mV/s) of an anatase TiO_2 mesoporous nanoparticle electrode in 0.5 M $LiClO_4$/acetonitrile. The arrows indicate scan direction.

Results and Discussion

Effect of Lithium on Electron Transport. Figure 2 displays a typical cyclic voltammogram of a TiO_2 mesoporous nanoparticle electrode in 0.5 M $LiClO_4$/acetonitrile. When the potential is scanned negatively, a cathodic peak, corresponding to lithium intercalation, is produced. Upon reversing the scan direction, an anodic peak, corresponding to the deintercalation (extraction) of the lithium ions is observed. Figure 3a shows a series of absorbance spectra of the TiO_2 electrode in the same electrolyte taken at different applied potentials, starting at 0 V (reference spectrum) and then measured at -1.2, -0.9, -0.6, -0.3, and 0 V. These spectra are consistent with previous observations.[44] As the potential is scanned from -1.2 to 0 V, the intensity of the absorption band of the intercalated film decreases progressively, corresponding to the deintercalation of lithium. In the spectral regime between the vertical dashed lines, the spectra exhibit a power-law dependence on wavelength, which is indicative of free electron absorption.[52,53] It is also seen that after the potential was cycled from 0 to -1.2 V, and

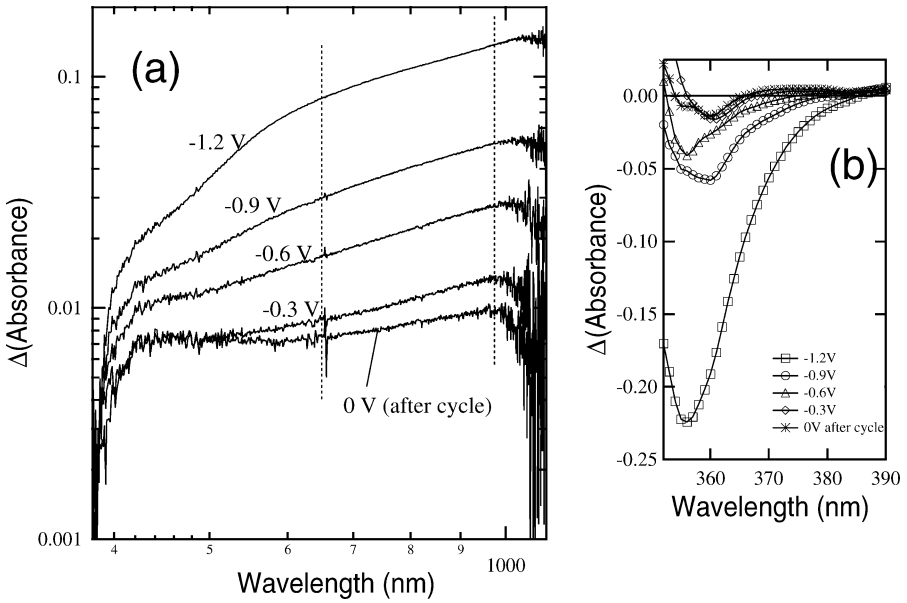

Figure 3. (a) Dependence of the absorbance difference spectra of an anatase TiO_2 mesoporous nanoparticle electrode in 0.5 M $LiClO_4$/acetonitrile on potential. The spectra were taken sequentially at potentials of 0 V (reference spectrum), −1.2, −0.9, −0.6, −0.3, and 0 V. In the spectral regime between the vertical dashed lines, the spectra exhibit a power-law dependence on wavelength. (b) Absorbance difference spectra dependence on potential in the vicinity of the band gap of anatase TiO_2.

then back to 0 V, residual coloration remains, which is indicative of trapped lithium in the TiO_2 film and the associated charge-compensating electrons.[45] Figure 3b displays the difference spectra in the vicinity of the band gap of anatase TiO_2 at various potentials in the cycle starting at −1.2 V and returning to 0 V. It can be seen that at more negative potentials increased absorbance loss (bleaching) and increased blue-shifting occurs relative to the conduction band excitation threshold of TiO_2 at 387 nm (3.2 eV). The observed absorption loss and spectral shift are attributed to the Moss-Burstein effect[54] resulting from the accumulation of charge-compensating electrons in the conduction band of TiO_2 associated with intercalated lithium. The presence of a small absorption loss at 360 nm upon completing the cycle is indicative of residual lithium in the TiO_2 film, which suggests that TiO_2 films in a lithium-containing electrolyte can be doped with lithium by cycling the potential.

The density of inserted Li in the TiO_2 film can be estimated from Figure 3. Optical absorption studies of Li intercalation in mesoporous anatase TiO_2 films have shown that in the solid solution regime (Li:TiO_2), corresponding to an inserted Li concentration below 5 atom %, the absorbance displays a power-law dependence on the wavelength indicative of quasi-free electrons.[44] At inserted Li concentration above 5 atom %, peaks appear in the absorbance spectrum[44] that signify the presence of localized electrons, corresponding to the transformation of Li:TiO_2 to lithium titanate (Li_xTiO_2). Thus, the power-law dependence of the absorbance on wavelength that is displayed in Figure 3 is indicative of the solid solution phase of lithium in the TiO_2 film, corresponding to a density of irreversibly inserted Li below 5 atom %. Further corroboration for the estimated density of irreversibly trapped Li in the TiO_2 films can be obtained by analyzing the coloration efficiency[44] of the Li insertion process; the coloration efficiency is a measure of the increase in absorbance at a particular wavelength per unit of Li charge density added to the film. Taking the coloration efficiency for the Li:TiO_2 phase at the wavelength of 725 nm to be 12 cm^2/C[44] and the absorbance increase at 0 V at the end of the voltage cycle to be about 8×10^{-3}, we estimate a density of irreversibly inserted Li of about 4×10^{18} cm^{-3} in a 10 μm thick film. This represents about 40 Li atoms per particle for a density of TiO_2 nanoparticles of ca. 10^{17} cm^{-3} (for a 10 nm particle radius).

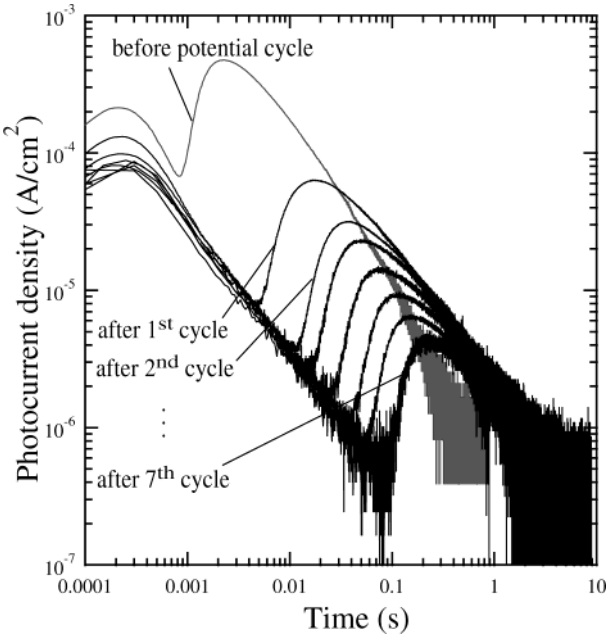

Figure 4. Photocurrent transients of a nonsensitized anatase TiO_2 mesoporous nanoparticle electrode in 0.5 M $LiClO_4$/acetonitrile in the absence of bias light. The cell was probed with 337 nm laser pulses incident at the outermost surface of the TiO_2 working electrode. The first transient was measured at 0 V before the first potential cycle was performed. Subsequent transients were measured at 0 V after cycling the potential of the electrode (6 mV/s) between 0 and −0.7 V for a progressive number of cycles.

Figure 4 shows photocurrent transients of a mesoporous TiO_2 electrode in 0.5 M $LiClO_4$/acetonitrile at 0 V vs Ag/AgCl. The cell was probed with 337 nm laser pulses, which were incident at the outermost surface of the TiO_2 working electrode. The UV laser pulse creates electron−hole pairs in the TiO_2 nanoparticles, some of which recombine, while others escape recombination because of the hole reaction with the solvent. The electrons that are left behind diffuse to the collecting

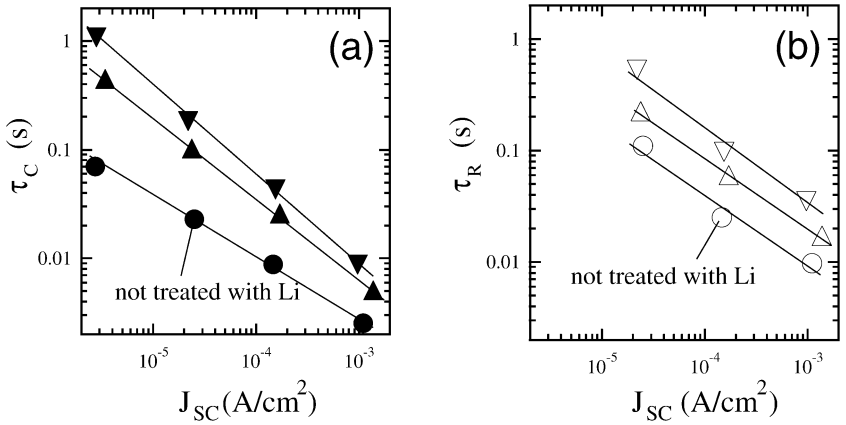

Figure 5. Effect of potential-induced lithium intercalation of TiO_2 nanoparticle electrodes on the collection time τ_C (a) (●, ▲, ▼) and recombination time τ_R (b) (○, △, ▽) of photocarriers for the DSSCs listed in Table 1. The circles represent a dye-sensitized TiO_2 nanoparticle electrode not exposed to a lithium solution (cell #1 of Table 1). Up-triangles (cell #3) represent TiO_2 electrodes in 0.5 M $LiClO_4$/acetonitrile that underwent 4 cycles (3 mV/s) between 0 V and −0.6, −0.8, −1.0, and −1.5 V before staining with the sensitizer. Down-triangles (cell #4) represent a cell made from a TiO_2 electrode in 0.5 M $LiClO_4$/acetonitrile that underwent 4 cycles (6 mV/s) between 0 V and −1.5V before staining with the sensitizer. In the assembled DSSCs, the electrolyte was 0.8 M C6DMII with 50 mM I_2 in methoxypropionitrile. The cells were probed with 532 nm laser pulses incident at the counter-electrode. The 680 nm bias light was incident on the cell from the collecting electrode side. J_{SC} corresponds to the short-circuit photocurrent induced by the bias light. The lines represent power-law fits.

electrode. The shapes of the photocurrent transients typify electron transport in TiO_2 films in the absence of bias illumination—namely, the presence of a peak after a time delay, corresponding to the collection of the main packet of electrons,[1,7] followed by a long dispersive (power-law) tail, which has been attributed to electron emission from deep traps.[28] The small peak at about 200 μs, which comprises less than 1% of the total collected charge, is due to charge carriers produced near or in the conducting oxide substrate by reflected and scattered light.[7] The photocurrent transient measured before the first voltage cycle represents the TiO_2 film containing the least amount of intercalated lithium. The other photocurrent transients were measured after cycling the potential of the electrode between 0 and −0.7 V for a progressive number of cycles. Although a quantitative evaluation of the amount of intercalated lithium was not feasible, it is expected that the density of intercalated lithium increases with the number of potential sweeps. Figure 4 shows that after just one potential cycle, electron transport slows dramatically, almost 1 order of magnitude. Subsequent potential cycles cause still slower arrival times of photogenerated electrons, indicating that increasingly larger amounts of intercalated lithium lead to progressively slower transport. After 7 cycles, the bulk of electrons arrive after a delay of about 0.2 s, which is 2 orders of magnitude slower than before lithium intercalation. Other researchers have observed a similar effect for lithium intercalation below 5 atom %[43,44,49] and have attributed it to electron scattering at lithium impurities.[44] When the first voltage cycle is between 0 and −1.5 V the arrival time of photogenerated electrons at the collector (not shown) is much longer than when the potential of the electrode is cycled seven times between 0 and −0.7 V. Therefore, a single voltage cycle between 0 and −1.5 V results in a residual Li density higher than that obtained after consecutive voltage cycles between 0 and −0.7 V.

To determine whether the photocharge density produced in the film by the 337 nm probe light could induce lithium intercalation, a TiO_2 nanoparticle electrode immersed in 0.5 M $LiClO_4$/acetonitrile at 0 V vs Ag/AgCl was subjected to 500 pulses of the 337 nm probe light. The photocurrent transient after the 500th pulse was identical to the one observed after the first pulse. Thus, the small density of photocharge introduced into film by the probe pulses is not sufficient to induce significant lithium insertion.

Figure 5 shows the effect of potential-induced lithium intercalation of TiO_2 nanoparticle electrodes on the collection and recombination times of photocarriers for DSSCs. The collection times for cells in which the TiO_2 electrodes in 0.5 M $LiClO_4$/acetonitrile were intercalated with Li by cycling the potential between 0 and −1.5 V in the dark before being stained with the sensitizer are considerably longer than the collection times for cells comprised of nonintercalated electrodes. This result indicates that lithium intercalation survives the subsequent steps of dye adsorption and cell assembly and that residual lithium in the dye-sensitized film slows electron transport markedly in a working solar cell. Figure 5a shows that increasing the amount of intercalated lithium in a film causes the collection time τ_C to depend more strongly on the short-circuit photocurrent (or incident light intensity). In the trap-limited electron transport model involving an exponential distribution of localized trap states, this dependence is expressed by the relation[7,23]

$$\tau_C \propto J_{SC}^{\alpha-1} \tag{4a}$$

where the parameter α is related to the steepness of the exponential trap-state distribution.[1,7,23]

Combining eq 4a with eqs 2 and 3 leads to relations between the short-circuit photocurrent, the photocharge density N, and the diffusion coefficient D.

$$N \propto J_{SC}^{\alpha} \tag{4b}$$

$$D \propto J_{SC}^{1-\alpha} \propto N^{(1-\alpha)/\alpha} \tag{4c}$$

Equations 4a−c have been described in detail elsewhere[1,7,23] but for simplicity are presented here as proportionalities. The parameter α in eqs 4a−c is related to the characteristic energy m_c of the exponential decay of the trap-state distribution by the equation[1,7,23]

$$m_c = kT/\alpha \tag{5}$$

where T is the absolute temperature and k is the Boltzmann constant. Thus, the change in α implies that the intercalation

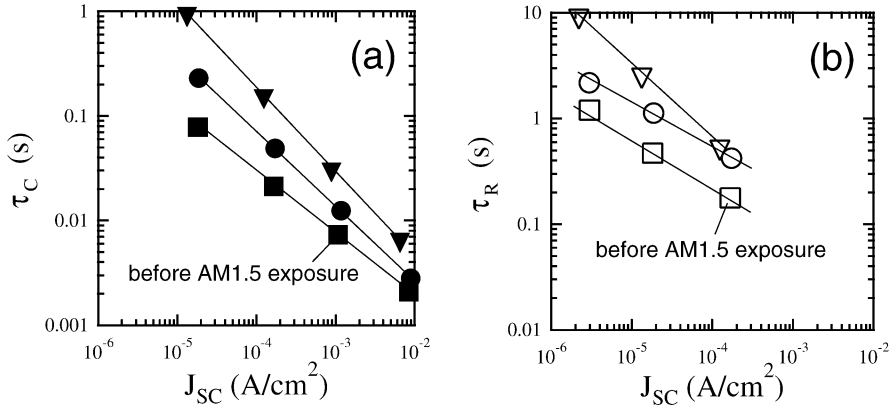

Figure 6. Effect of light-induced lithium intercalation of a dye-sensitized TiO_2 nanoparticle electrode on the collection time τ_C (a) (■, ●, ▼) and recombination time τ_R (b) (□, ○, ▽) of photocarriers. The squares (cell #5 in Table 1) represent the DSSC before exposure to AM1.5 equivalent light intensity. The circles (cell #5) represent the same cell after exposure to AM1.5 equivalent light intensity at open circuit for 30 min before the photocurrent transient measurement. Down-triangles (cell #5) represent the cell after exposure to AM1.5 for a total of 3 1/2 h at open circuit. The electrolyte was 0.8 M LiI with 50 mM I_2 in methoxypropionitrile. The cell was probed with 532 nm laser pulses incident at the counter electrode. The 680 nm bias light was incident on the cell from the collecting electrode side. J_{SC} corresponds to the short-circuit photocurrent induced by the bias light. The lines represent power-law fits.

of lithium affects the trap-state distribution. This issue is discussed in more detail below.

A comparison of Figures 5a and 5b reveals that the increase of the electron collection time τ_C, corresponding to a decrease of the electron diffusion coefficient, in the Li-doped samples is accompanied by a comparable increase of the recombination lifetime τ_R. This observation suggests that electron diffusion and recombination are causally linked.

Figure 6 shows the effect of light-induced lithium intercalation of a dye-sensitized TiO_2 nanoparticle electrode (cell #5; Table 1) on the collection time and recombination time of electrons. The DSSC was filled with 0.8 M LiI/0.05 M I_2 and subsequently exposed to AM1.5 light at open circuit for periods of 30 min and then 3 h. After each illumination period, the collection and recombination times were measured. Figure 6 shows that both the transport and recombination times become proportionally slower with longer illumination periods. Inasmuch as the same effect is observed when Li intercalation is induced by an applied potential (Figure 5), we conclude that lithium intercalates into sensitized TiO_2 films when Li^+ is present in the electrolyte under normal illumination conditions of the cell. Furthermore, when the exposure time of the cell to AM1.5 light is increased from 0 min to $3^1/_2$ h, the power-law exponent of the curves increases markedly. The charge transport kinetics undergoes a similar change (not shown) when the TiO_2 electrode of a DSSC filled with 0.8 M LiI/0.05 M I_2 in methoxypropionitrile is subjected to a voltage of -0.7 V for several minutes in the dark. This is about the same open-circuit voltage produced by the cell under AM 1.5 illumination. The effect of lithium intercalation to slow both transport and recombination persists for at least several days. These results indicate that lithium intercalation (reaction 1) occurs when electrons are injected either from the back contact under applied potential or from the excited state of the dye. Thus, the accumulation of electrons in TiO_2 is requisite for lithium intercalation. To our knowledge, this is the first evidence that lithium intercalates into dye-sensitized TiO_2 films at solar light intensities.

Figure 7 shows the effect of (a) potential-induced and (b) light-induced lithium intercalation of TiO_2 nanoparticle electrodes on the diffusion coefficient of photocarriers in DSSCs over the same range of light intensity. The diffusion coefficient and the photoinduced steady-state charge density at short circuit were determined from the characteristic times for electron diffusion and eqs 2 and 3, respectively. Figure 7a was constructed from the data in Figure 5a (along with an additional data set). It can be seen in Figure 7a that that the logarithmic slope of the power-law relation between D and N ($(1 - \alpha)/\alpha$ (eq 4c)) increases from a value of 1.3 for a TiO_2 electrode without intercalated Li (cell #1) to a value of 4.3 for a TiO_2 electrode with a large density of intercalated Li (cell #4), which implies (eq 4b) that the dependence of photoinjected charge on light intensity becomes weaker upon Li intercalation. Thus, as the amount of intercalated Li increases, the electron diffusion coefficient becomes more dependent on the amount of photoinjected charge, while the photoinjected charge becomes less dependent on the light intensity.

Figure 7b shows an even stronger dependence of the diffusion coefficient on the photocharge density as a function of light-induced intercalated Li. A striking result of the photocurrent transient measurements is the dependence of the diffusion coefficient on photocharge density when the DSSC is exposed to AM1.5 illumination for $3^1/_4$ days. In this case, the power-law exponent of the D vs N curve ($(1 - \alpha)/\alpha$ (eq 4c)) was 17. The relatively high value of this slope implies that α is close to zero and that the photocharge density (eq 4b), therefore, varies relatively little with light intensity. To determine whether the decrease of the diffusion coefficient is attributable to factors other than light-induced Li intercalation (e.g., intercalation of protons owing to the presence of the protonated dye or trace water), studies were performed on DSSCs that did not contain Li. It was found that when a cell contained a Li-based electrolyte and was exposed to AM1.5 light for 5 h, the electron diffusion coefficient decreased by at least 3 orders of magnitude, whereas when it contained a $C6DMI^+$-based electrolyte under the same illumination condition, the electron diffusion coefficient decreased by less than 1 order of magnitude. Presumably, in the latter case, the slower transport was due to proton intercalation. These studies ruled out the possibility that factors other than lithium intercalation can account for the observed decrease in the diffusion coefficient.

Figure 7 also demonstrates that the electron diffusion coefficient in DSSCs exhibits a power-law dependence on photocharge at all concentration levels of intercalated lithium. This power-law dependence is consistent with an exponential trap-state distribution[1,7,23,32] described by eqs 4c and 5. Figure 7 shows that m_c (eq 5) increases from 61 to 400 meV with

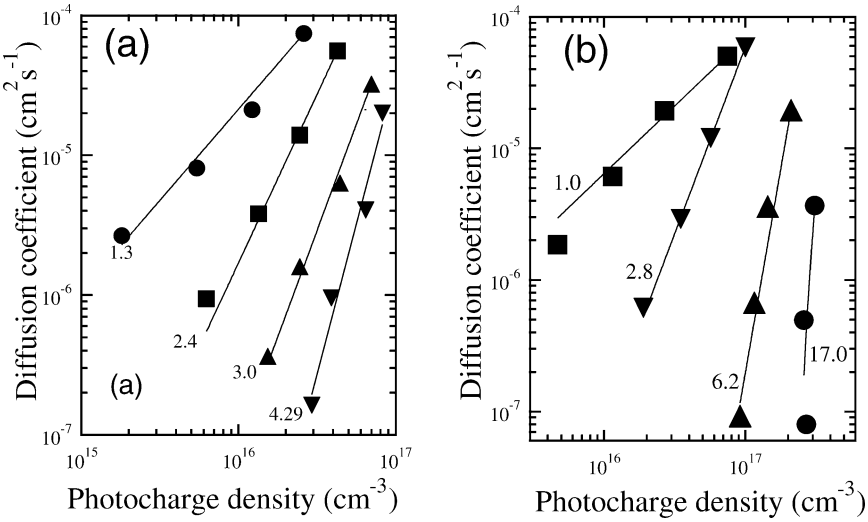

Figure 7. Effect of potential-induced (a) and light-induced (b) lithium intercalation of TiO_2 nanoparticle electrodes on the diffusion coefficient of photocarriers for the DSSCs listed in Table 1. (a) The same conditions and symbols (●, ▲, ▼) described in Figure 5 for cells #1, #3, and #4 were used. The squares (cell #2) represent a TiO_2 electrode that underwent 1 cycle between 0 and −1.3 V before being stained with the sensitizer. In the assembled DSSCs, the electrolyte was 0.8 M C6DMII with 50 mM I_2 in methoxypropionitrile. (b) The squares (cell #6 in Table 1) represent a 4-*tert*-butylpyridine-treated dye-sensitized TiO_2 nanoparticle electrode not exposed to AM1.5 light before the transient measurements. The other symbols represent the same dye-sensitized TiO_2 nanoparticle electrode (cell #6) after it was exposed to AM1.5 light for, respectively, a total of 30 min (▼), $5^1/_2$ h (▲), and 3 days $5^1/_2$ h (●) before the transient measurements. The electrolyte used in the cell in this case was 0.8 M LiI with 50 mM I_2 in methoxypropionitrile. The lines represent power-law fits (eq 4c) to the data, and their labels indicate the values of the logarithmic slope $(1 - \alpha)/\alpha$ obtained by the best fit.

increasing lithium insertion levels. The large increase of m_c is ascribed to the widening of the exponential conduction band tail (by a factor of 6.5) resulting from disorder induced by randomly placed lithium defects in TiO_2.[55]

Mechanism for Transport-Limited Recombination. Figures 5 and 6 show that the characteristic times for diffusion and recombination increase by comparable amounts when the TiO_2 films are interacted with Li. These results suggest that recombination is a diffusion-limited process in DSSCs. A key assumption here is that trap states induced by Li insertion only alter the diffusion of electrons and have no significant effect on interfacial electron transfer to the redox couple (recombination). For this case, it follows that the characteristic time for recombination increases as a result of slower electron diffusion and therefore that recombination is diffusion limited. In the following, we present a model for diffusion-limited recombination and discuss the underlying assumptions.

Sometime ago we reported that the rate of recombination in dye-sensitized solar cells is approximately second order with respect to the electron concentration in the film.[36,56] The second-order nature of the reaction can be explained by either scheme 1 (reactions 6−8)[36,56] or scheme 2 (reactions 6−7 and 9):[32,57]

$$I_3^- \overset{K_4}{\longleftrightarrow} I_2 + I^- \tag{6}$$

$$e^- + I_2 \xrightarrow{k_5} I_2^{\bullet -} \tag{7}$$

$$2I_2^{\bullet -} \rightarrow I_3^- + I^- \tag{8}$$

$$I_2^{\bullet -} + e^- \rightarrow 2I^- \tag{9}$$

In both schemes, I_3^- exists in chemical equilibrium with iodide ions in solution and molecular iodine associated with the TiO_2 surface (reaction 6). Injected electrons from TiO_2 are presumed to reduce I_2 to the $I_2^{\bullet -}$ radical anion, which reacts further via reaction 8 (Scheme 1) or reaction 9 (Scheme 2). Previously, either reaction 8[36,56] or reaction 9[32,57] has been assumed to be rate limiting. However, to account for diffusion-limited recombination results, it is necessary to assume that the electron-capture reaction 7 is rate limiting. With this assumption, the overall rate of recombination R for reactions 6 and 7 can be expressed as

$$R = K_4 k_5 \frac{[I_3^-]}{[I^-]} N \tag{10}$$

where N is the electron concentration.

The equilibrium constant of reaction 6 (K_4) is estimated to be 10^{-10} mol/cm[3,32] which leads to a steady-state concentration of molecular iodine of 10^{13} cm^{-3} for initial concentrations of 0.8 M I^- and 0.05 M I_2. Assuming that every I_2 species produced by reaction 6 is a potential recombination site (via reaction 7), the concentration of potential recombination sites is 4 orders of magnitude lower than the density of TiO_2 nanoparticles (ca. 10^{17} cm^{-3} for 10 nm radius particles). Computer simulations of electron transport in random nanoparticle films[58] show that an electron visits about 10^6 nanoparticles on average in a 10 μm thick film before reaching the collecting electrode. Taking into account that an electron visits 10^4 nanoparticles before encountering a potential recombination site, it is plausible that the value of k_5 (reaction 7) is limited by the interparticle transport of the electron to the recombination site. Taking k_5 to be proportional to the electron diffusion coefficient D, the rate of recombination (eq 10) can be written as

$$R \propto DN \tag{11}$$

Because D depends on N (eq 4c), the rate of recombination (eq 11) depends nonlinearly on N, which agrees with experimental observations.[19,32,36] Assuming pseudo-first-order kinetics, i.e., $R = N/\tau_R$, it is found with the aid of eq 2 that the time constant

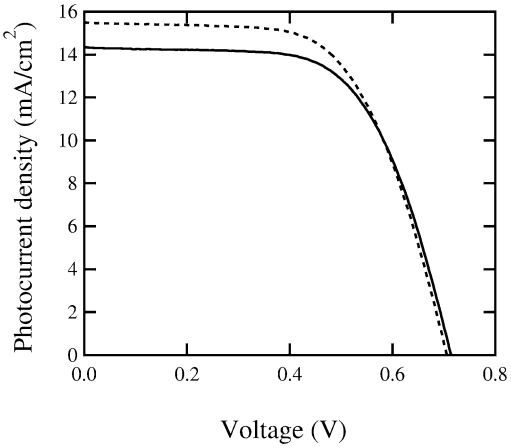

Figure 8. Effect of Li intercalation of TiO_2 nanoparticle electrodes on the performance of DSSCs under simulated AM1.5 equivalent light. The dashed line represents a cell incorporating a dye-sensitized TiO_2 nanoparticle electrode not exposed to a lithium solution (cell #1 of Table 1). The solid line (cell #4) represents a cell made from a TiO_2 electrode in 0.5 M $LiClO_4$/acetonitrile that underwent 4 cycles (6 mV/s) between 0 V and −1.5 V before staining with the sensitizer. The electrolyte was 0.8 M C6DMII with 50 mM I_2 in methoxypropionitrile.

for recombination τ_R is given by the expression

$$\tau_R \propto \frac{1}{D} \propto \tau_C \tag{12}$$

Equation 12 implies that a change in the diffusion time results in an equal change in the recombination time. This result is in accord with the experimental observations above, suggesting that electron diffusion limits recombination.

Solar Cell Performance. Because lithium-containing electrolytes are used commonly for DSSCs and Li insertion affects both the collection and recombination of electrons, it is important to determine whether Li intercalation influences cell performance. Figure 8 compares the PV response of nonintercalated and intercalated DSSCs containing the same redox electrolyte. The solar cells exhibit almost the same open-circuit photovoltages (ca. 0.71 V) and comparable short-circuit photocurrent densities (15.5 mA/cm^2 for the nonintercalated cell and 14.3 mA/cm^2 for the Li intercalated cell). These results indicate that the PV characteristics of the DSSC are largely unaffected by lithium intercalation. Because the characteristic time of recombination changes almost in unison with the electron diffusion time, lithium intercalation has only a small effect on the charge collection efficiency[19] and therefore on the short-circuit photocurrent density. In the absence of a significant band-edge shift, the open circuit voltage V_{OC} depends on the recombination rate constant of electrons with the redox couple.[36] Other parameters (e.g., the absorbed photon flux[36]) affecting V_{OC} are presumably unchanged by Li insertion. The diffusion-limited recombination model predicts that a decrease of the electron diffusion coefficient leads to a small increase of V_{OC} ($V_{OC} \propto \ln(1/k_5) \propto \ln(1/D)$).[56] Furthermore, because the decrease of D is relatively small at light intensities close to 1 sun (Figures 5 and 6), no appreciable change of V_{OC} is observed (Figure 8). The important conclusion that these results suggest is that the solar cell performance will not be significantly improved by enhancing the electron transport rate (i.e., the diffusion coefficient).

Conclusions

Photocurrent and photovoltage transient measurements of sensitized and nonsensitized TiO_2 films show that electron transport limits recombination in dye-sensitized nanoparticle solar cells under their normal operating conditions. This conclusion is based on the effect that lithium intercalation has on the transport dynamics and recombination kinetics in sensitized TiO_2 nanoparticle films. When Li^+ is present in the electrolyte, lithium intercalates irreversibly into dye-sensitized TiO_2 films at open circuit (ca. −0.7 V) under normal solar light intensities. The characteristic times for electron diffusion and recombination become proportionately slower as the Li density in the films increases, indicating that electron transport limits the recombination of electrons with redox species at the TiO_2/liquid electrolyte interface. The electron diffusion coefficient in dye-sensitized solar cells exhibits a power-law dependence on photocharge at all concentrations of lithium insertion in the TiO_2 film, which is ascribed to widening of the exponential conduction band tail owing to additional disorder produced by randomly placed lithium defects. While the electron diffusion coefficient depends strongly on photocharge density, the photocharge density changes relatively little with light intensity. Although lithium intercalation is shown to occur during the normal operation of the cell, its effect on the cell's PV characteristics is insignificant. These results suggest that increasing the electron transport rate will not significantly improve the solar cell performance.

Acknowledgment. This work was supported by the Office of Science, Division of Chemical Sciences, and the Office of Utility Technologies, Division of Photovoltaics, U. S. Department of Energy, under contract DE-AC36-99GO10337.

References and Notes

(1) Kopidakis, N.; Schiff, E. A.; Park, N.-G.; van de Lagemaat, J.; Frank, A. J. *J. Phys. Chem. B* **2000**, *104*, 3930.
(2) van de Lagemaat, J.; Park, N.-G.; Frank, A. J. *J. Phys. Chem. B* **2000**, *104*, 2044.
(3) Schwarzburg, K.; Willig, F. *J. Phys. Chem. B* **1999**, *103*, 5743.
(4) Bisquert, J.; Garcia-Belmonte, G.; Fabregat-Santiago, F. *J. Solid State Electrochem.* **1999**, *3*, 337.
(5) Papageorgiou, N.; Grätzel, M.; Infelta, P. P. *Sol. Energy Mater. Sol. Cells* **1996**, *44*, 405.
(6) Zaban, A.; Meier, A.; Gregg, B. *J. Phys. Chem. B* **1997**, *101*, 7985.
(7) van de Lagemaat, J.; Frank, A. J. *J. Phys. Chem. B* **2001**, *105*, 11194.
(8) Nakade, S.; Kambe, S.; Kitamura, T.; Wada, Y.; Yanagida, S. *J. Phys. Chem. B* **2001**, *105*, 9150.
(9) Nistér, D.; Keis, K.; Lindquist, S.-E.; Hagfeldt, A. *Sol. Energy Mater. Sol. Cells* **2002**, *73*, 411.
(10) Solbrand, A.; Lindström, H.; Rensmo, H.; Hagfeldt, A.; Lindquist, S.-E. *J. Phys. Chem. B* **1997**, *101*, 2514.
(11) Schwarzburg, K.; Willig, F. *Appl. Phys. Lett.* **1991**, *58*, 2520.
(12) Cao, F.; Oskam, G.; Meyer, G. J.; Searson, P. C. *J. Phys. Chem.* **1996**, *100*, 17021.
(13) Solbrand, A.; Henningsson, A.; Södergren, S.; Lindström, H.; Hagfeldt, A.; Lindquist, S.-E. *J. Phys. Chem. B* **1999**, *103*, 1078.
(14) Dittrich, T. *Phys. Status Solidi A* **2000**, *182*, 447.
(15) Dittrich, T.; Weidmann, J.; Timoshenko, V. Y.; Petrov, A. A.; Koch, F.; Lisachenko, M. G.; Lebedev, E. *Mater. Sci. Eng. B* **2000**, *69*−*70*, 489.
(16) Dittrich, T.; Lebedev, E. A.; Weidmann, J. *Phys. Status Solidi A* **1998**, *165*, R5.
(17) Dloczik, L.; Ileperuma, O.; Lauermann, I.; Peter, L. M.; Ponomarev, E. A.; Redmond, G.; Shaw, N. J.; Uhlendorf, I. *J. Phys. Chem. B* **1997**, *101*, 10281.
(18) Kambili, A.; Walker, A. B.; Qiu, F. L.; Fisher, A. C.; Savin, A. D.; Peter, L. M. *Physica E* **2002**, *14*, 203.
(19) Schlichthörl, G.; Park, N.-G.; Frank, A. J. *J. Phys. Chem. B* **1999**, *103*, 782.
(20) Vanmaekelbergh, D.; de Jongh, P. E. *Phys. Rev. B* **2000**, *61*, 4699.
(21) de Jongh, P. E.; Vanmaekelbergh, D. *Phys. Rev. Lett.* **1996**, *77*, 3427.
(22) de Jongh, P. E.; Vanmaekelbergh, D. *J. Phys. Chem. B* **1997**, *101*, 2716.
(23) van de Lagemaat, J.; Frank, A. J. *J. Phys. Chem. B* **2000**, *104*, 4292.

(24) Fabregat-Santiago, F.; Garcia-Belmonte, G.; Bisquert, J.; Zaban, A.; Salvador, P. *J. Phys. Chem. B* **2002**, *106*, 334.
(25) Kern, R.; Sastrawan, R.; Ferber, J.; Stangl, R.; Luther, J. *Electrochim. Acta* **2002**, *47*, 4213.
(26) Bisquert, J.; Garcia-Belmonte, G.; Fabregat-Santiago, F.; Ferriols, N. S.; Bogdanoff, P.; Pereira, E. C. *J. Phys. Chem. B* **2000**, *104*, 2287.
(27) Gregg, B. A.; Pichot, F.; Ferrere, S.; Fields, C. L. *J. Phys. Chem. B* **2001**, *105*, 1422.
(28) Könenkamp, R. *Phys. Rev. B* **2000**, *61*, 11057.
(29) Könenkamp, R.; Wahi, A.; Hoyer, P. *J. Phys. Chem.* **1993**, *97*, 7328.
(30) Dittrich, T.; Weidmann, J.; Koch, F.; Uhlendorf, I.; Lauermann, I. *Appl. Phys. Lett.* **1999**, *75*, 3980.
(31) Nelson, J. *Phys. Rev. B* **1999**, *59*, 15374.
(32) Fisher, A. C.; Peter, L. M.; Ponomarev, E. A.; Walker, A. B.; Wijayantha, K. G. U. *J. Phys. Chem. B* **2000**, *104*, 949.
(33) Haque, S. A.; Tachibana, Y.; Klug, D. R.; Durrant, J. R. *J. Phys. Chem. B* **1998**, *102*, 1745.
(34) Haque, S. A.; Tachibana, Y.; Willis, R. L.; Moser, J. E.; Grätzel, M.; Klug, D. R.; Durrant, J. R. *J. Phys. Chem. B* **2000**, *104*, 538.
(35) Nelson, J.; Haque, S. A.; Klug, D. R.; Durrant, J. R. *Phys. Rev. B* **2001**, *63*, 205321.
(36) Schlichthörl, G.; Huang, S. Y.; Sprague, J.; Frank, A. J. *J. Phys. Chem. B* **1997**, *101*, 8141.
(37) Dittrich, T.; Duzhko, V.; Kock, F.; Kytin, V.; Rappich, J. *Phys. Rev. B* **2002**, *65*, 155319.
(38) Enright, B.; Redmond, G.; Fitzmaurice, D. *J. Phys. Chem.* **1994**, *98*, 6195.
(39) Liu, Y.; Hagfeldt, A.; Xiao, X.-R.; Lindquist, S.-E. *Sol. Energy Mater. Sol. Cells* **1998**, *55*, 267.
(40) Park, N.-G.; Chang, S.-H.; van de Lagemaat, J.; Kim, K.-J.; Frank, A. J. *Bull. Korean Chem. Soc.* **2000**, *21*, 985.
(41) Kavan, L.; Grätzel, M.; Rathousk×c6, J.; Zukal, A. *J. Electrochem. Soc.* **1996**, *143*, 394.
(42) Kavan, L.; Kratochvilová, K.; Grätzel, M. *J. Electroanal. Chem.* **1995**, *394*, 93.
(43) van de Krol, R.; Goossens, A.; Meulenkamp, E. A. *J. Electrochem. Soc.* **1999**, *146*, 3150.
(44) van de Krol, R.; Goossens, A.; Meulenkamp, E. A. *J. Appl. Phys.* **2001**, *90*, 2235.
(45) van de Krol, R.; Goossens, A.; Schoonman, J. *J. Phys. Chem. B* **1999**, *103*, 7151.
(46) Lindström, H.; Södergren, S.; Solbrand, A.; Rensmo, H.; Hjelm, J.; Hagfeldt, A.; Lindquist, S.-E. *J. Phys. Chem. B* **1997**, *101*, 7710.
(47) Lindström, H.; Södergren, S.; Solbrand, A.; Rensmo, H.; Hjelm, J.; Hagfeldt, A.; Lindquist, S.-E. *J. Phys. Chem. B* **1997**, *101*, 7717.
(48) Södergren, S.; Siegbahn, H.; Rensmo, H.; Lindström, H.; Hagfeldt, A.; Lindquist, S.-E. *J. Phys. Chem. B* **1997**, *101*, 3087.
(49) Zachau-Christiansen, B.; West, K.; Jacobsen, T.; Atlung, S. *Solid State Ionics* **1988**, *28*−*30*, 1176.
(50) Park, N.-G.; van de Lagemaat, J.; Frank, A. J. *J. Phys. Chem. B* **2000**, *104*, 8989.
(51) van de Lagemaat, J.; Benkstein, K. D.; Frank, A. J. *J. Phys. Chem. B* **2001**, *105*, 12433.
(52) Pankove, J. I. *Optical processes in semiconductors*; Dover Publications: New York, 1971.
(53) Szczepankiewicz, S. H.; Moss, J. A.; Hoffmann, M. R. *J. Phys. Chem. B* **2002**, *106*, 2922.
(54) Enright, B.; Fitzmaurice, D. *J. Phys. Chem.* **1996**, *100*, 1027.
(55) Silver, M.; Pautmeier, L.; Bässler, H. *Sol. State Commun.* **1989**, *72*, 177.
(56) Huang, S. Y.; Schlichthörl, G.; Nozik, A. J.; Grätzel, M.; Frank, A. J. *J. Phys. Chem. B* **1997**, *101*, 2576.
(57) Bauer, C.; Boschloo, G.; Mukhtar, E.; Hagfeldt, A. *J. Phys. Chem. B* **2002**, *106*, 12693.
(58) Benkstein, K. D.; Kopidakis, N.; van de Lagemaat, J.; Frank, A. J. *J. Phys. Chem. B* **2003**, *107*, 7759.